LAWRENCE
LIVERMORE
NATIONAL
LABORATORY

UCRL-TR-228230

Laser-Matter Interactions with a 527 nm Drive

Siegfried Glenzer, Christoph Niemann, Pamela Witman, Paul Wegner, Daniel Mason, Christoph Haynam, Thomas Parham, Phil Datte

February 21, 2007

This work was performed under the auspices of the U.S. Department of Energy by University of California, Lawrence Livermore National Laboratory under Contract W-7405-Eng-48.

NIF Program: LDRD-ER Final Report

Laser-Matter Interactions with a 527 nm Drive

Tracking No.: 03-ERD-071

Principal Investigator:	Siegfried Glenzer Phone: 2-7409	(ICF-NIF) Mail Code: L-399
Co-investigators:	Christoph Niemann (NIF) Pamela Witman (NIF) Paul Wegner (NIF) Daniel Mason (Engr)	Christoph Haynam (NIF) Thomas Parham (CMS) Phil Datte (Engr)

Objectives:
The primary goal of this Exploratory Research is to develop an understanding of laser-matter interactions with 527-nm light (2ω) for studies of interest to numerous Laboratory programs including inertial confinement fusion (ICF), material strength, radiation transport, and hydrodynamics. In addition, during the course of this work we will develop the enabling technology and prototype instrumentation to diagnose a high fluence laser beam for energy, power, and near field intensity profile at 2ω.

Summary
Through this Exploratory Research we have established an extensive experimental and modeling data base on laser-matter interaction with 527 nm laser light (2ω) in plasma conditions of interest to numerous Laboratory programs. The experiments and the laser-plasma interaction modeling using the code pF3D have shown intensity limits and laser beam conditioning requirements for future 2ω laser operations and target physics experiments on the National Ignition Facility (NIF). These findings have set requirements for which present radiation-hydrodynamic simulations indicate the successful generation of relevant pressure regimes in future 2ω experiments. To allow these experiments on the NIF, optics and optical mounts were prepared for the 18mm Second Harmonic Generation Crystal (SHG crystal) that would provide the desired high conversion efficiency from 1ω to 2ω. Supporting experimental activities on NIF included high-energy 1ω shots at up to 22kJ/beamline (4MJ full NIF 1ω equivalent energy) that demonstrated, in excess, the 1ω drive capability of the main laser that is required for 2ω operations. Also, a very extensive 3ω campaign was completed (see "The National Ignition Facility Laser Performance Status" UCRL-JRNL-226553) that demonstrated that not only doubling the laser, but also tripling the laser (a much more difficult and sensitive combination) met our model predictions over a wide range of laser bandwidths and focal spot modification conditions. We have inferred that since we have successful modeled the 3ω performance that our 2ω model is also validated.

Introduction
LLNL has a long history of using laser light to probe increasingly higher regimes of pressure, temperature, and strain rate in matter, first with light at 1053 nm (1ω) and more recently with the NOVA and OMEGA lasers at 351 nm (3ω). In experiments using 3ω light, laser performance favor higher power at lower fluence where operation is limited by the B integral in the laser amplifiers. This ER has, using 2ω light, performed new studies of laser-plasma interactions to higher energies and higher fluences where higher damage thresholds for optics at 2ω allow greater energy extraction from the laser amplifiers. From a fundamental science point of view, the potentially increased available energy for experiments at 2ω allows potentially more robust ignition, potentially increased pressure for a given strain rate for material dynamics experiments and significant simplification of experiments due to the reduction of unconverted light in the target chamber for a wide variety of experiments. In addition, 2ω potentially allows a significant enhancement of the operating laser performance during the period up to full NIF.

Our program of work for this ER has met the following main goals:

- Perform experiments with 2ω on appropriate facilities to resolve important scientific questions relating to laser-plasma interactions, laser-target coupling, preheat and hohlraum filling, and to gain a better understanding of the advantages and limitations of 2ω illumination relative to 3ω.
- Design and prototype laser diagnostics for operations at 2ω.

In the following sections we will discuss the motivation for this work

Motivation:
From the standpoint of optimizing the laser driver, green light has several advantages: the energy delivered to target is greater than for blue light (3ω) because of greater conversion efficiency from the fundamental wavelength, the contrast ratio in the laser pulse shape can be higher, optical damage thresholds are larger, the laser pulse bandwidth is wider, and there is also less unconverted stray light to contend with in the chamber. One of the original motivations for using shorter wavelength light was to reduce the levels of hot electrons and scattered light produced by laser-plasma instabilities (LPI); going to longer wavelength generally means larger instability levels since the instability thresholds scale with $I\lambda^2$. Beam smoothing techniques, developed in recent years and tested in 3ω experiments, have been shown to be effective in controlling laser-plasma instabilities. These techniques are also applicable at 2ω and should provide similar benefit.

Performing experiments using laser light at 2ω will benefit LLNL in three important ways. First, it will significantly enhance our ability to support LLNL missions related to National Security and, in particular, the science-based Stockpile Stewardship Program (SSP). Secondly, from the point of view of fundamental science, the potential of significantly greater energy delivered onto target at 2ω enables a wide variety of experiments that scale strongly with energy (Fig. 1). In particular, five key stockpile stewardship programs would significantly benefit from 2ω drive: ignition, material dynamics, properties of special nuclear materials, x-ray sources for effects testing, and hydrodynamics. We discuss these in more detail below:

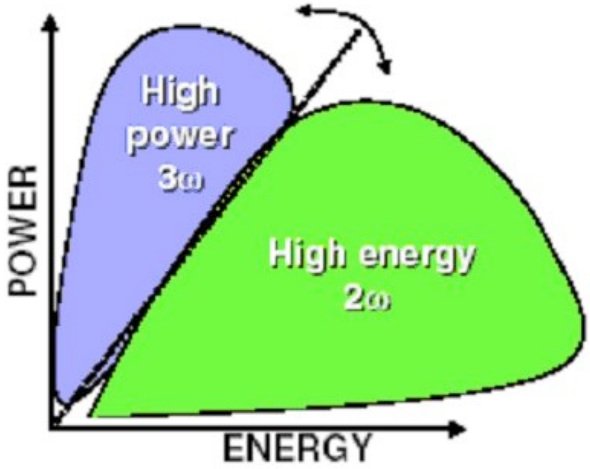

Figure 1. Regimes of beneficial laser performance 2ω versus 3ω.

Ignition

The NIF laser beams have the potential to drive capsules absorbing far more energy than we originally envisioned in 1991; see figure 2. The actual degree to which 2ω has the potential to drive a larger capsule than 3ω depends upon the degree to which optics can resist damage at 2ω vs. 3ω. Currently it appears that 2ω would allow a factor of two or more of fluence than 3ω. Consequently NIF, operating at 2ω may be able to drive a capsule which absorbs two or more times the energy than it would at 3ω, if the target physics worked out favorably. There is, however, a significantly greater uncertainty in the laser-target coupling with green light, due to laser plasma interactions (LPI). It was essential that we these LPI uncertainties have been addressed in new experiments at the Omega laser facility and on early NIF planning, to first assess the viability of using 2ω for ignition and then, if it looks plausible, optimize the implementation for ignition designs.

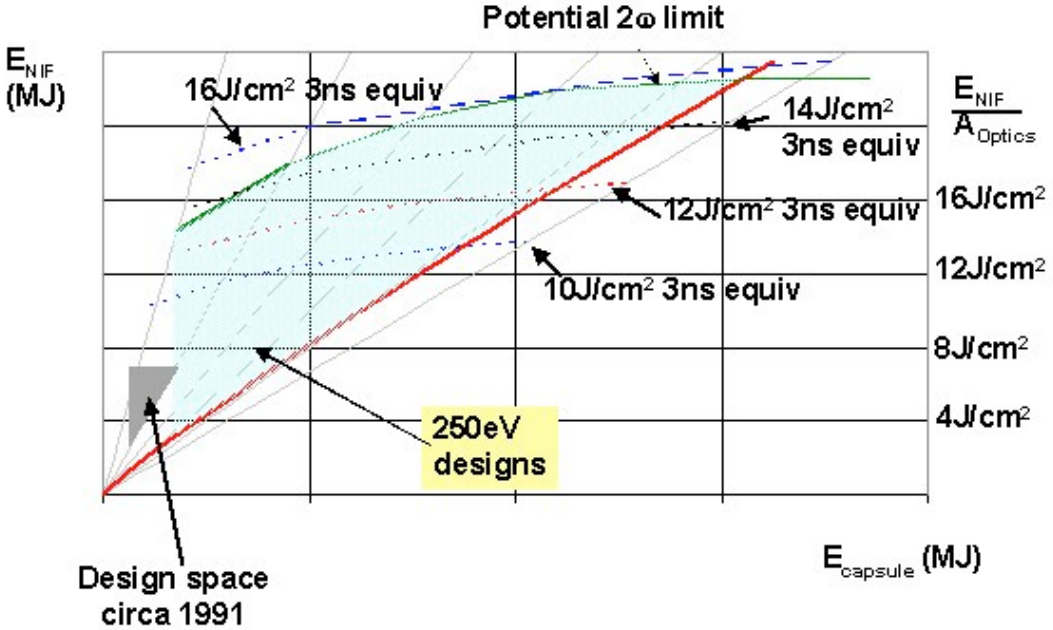

Figure 2. NIF energy absorbed by an ignition target vs. the x-ray energy absorbed by an ignition capsule

Material Dynamics

In the area of material dynamics, the increased energy at 2ω has two significant impacts. First, for a given strain rate, the isentropic pressure that is accessible on NIF using a plasma piston driver is ~ 30% higher compared to 3ω at the highest pressure ranges (Fig. 3). Secondly, at lower pressures, investigation of grain size effects requires thick samples, which in turn require long laser pulses. The additional energy afforded by long pulse 2ω on NIF will allow thicker samples at higher pressures. This requires both 2ω operation and conversion crystals optimized for long pulse operation. There are uncertainties in both the 2ω coupling to the target for long pulses as well as preheat generation from 2ω that could melt the target prematurely.

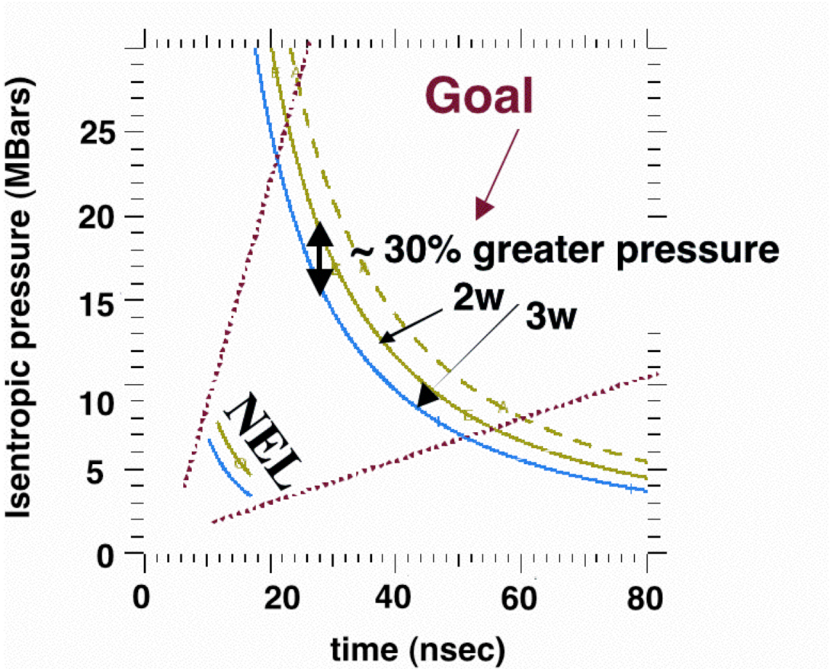

Figure 3. Plotted is the isentropic pressure achievable using 2ω compared to 3ω on NIF. In addition to ~30% greater pressure for a given strain rate using 2ω, the margin for accessing 20 pressures of Mbars and higher is greater for 2ω, as shown in the colored regions.

Special Nuclear Materials

One potential and important use of NIF in support of stockpile stewardship is to conduct experiments that study the material properties of special nuclear materials (SNM). To field experiments with SNM will require a containment vessel. Based on the conceptual designs, major cost drivers are the size of the containment vessel and the ability to insert it into the NIF target chamber without major modifications to the target chamber. With 2ω operation and using an optic to absorb much of the unconverted 1ω light, the chamber design, while difficult, is greatly simplified compared to 3ω. With 3ω operation, significant complexities are introduced because both the unconverted 1ω and 2ω light will propagate into the containment chamber and have a resultant focus near the containment vessel wall. Increasing the chamber size results in a chamber that is too large to fit through the existing ports. Operation at 3ω may well preclude the

practical use of SNM on NIF, and thus 2ω would allow a practical path towards a unique capability on NIF.

Effects

Another area is the generation of x-ray sources for effects testing. A traditional metric of a facility's utility for Nuclear Weapons Effects Testing (NWET) is the "fluence area" product, a quantity that scales linearly with multi-keV x-ray production. Simulations, corroborated by experiments, indicate that green light is as good as, or slightly better than, 3ω light for efficiently producing multi-keV x-rays. If green light provides significantly more laser energy than blue, the resulting increase in x-ray fluence area will be beneficial for NWET. Increased production of multi-keV x-rays is of direct benefit to HED physics experiments due to the ability to produce large area backlighting and to deeply preheat experimental packages.

Hydrodynamics

The major advantage of using 2ω for hydrodynamic experiments is a tremendous simplification of the experimental geometry and reduction of risk in its implementation. A typical hydrodynamics experiment has a target driven by a main set of laser beams and an x-ray backlighter driven by another set of beams. Because of unconverted light on NIF, shields are required to prevent unconverted light from hitting the targets and the backlighters. Operation at 2ω would eliminate most of the unconverted light from the target chamber, greatly simplifying the execution of these types of experiments. Figure 4 illustrates the unconverted light for NEL for a planar hydrodynamics experiment. An additional benefit of 2ω would be longer pulse drives, which would eliminate the need to stagger beams in time.

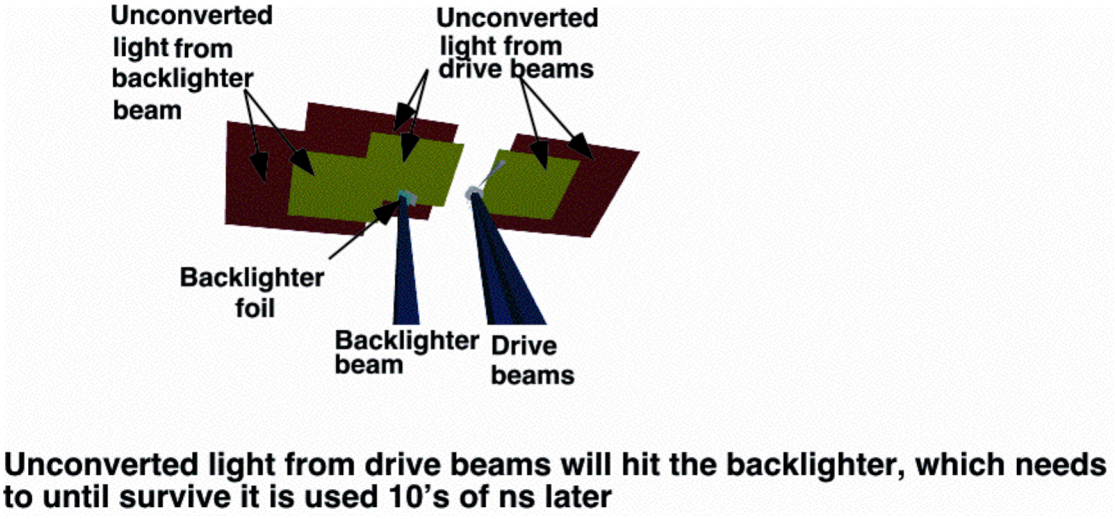

Figure 4. In the typical hydrodynamic target geometry using 3ω light, shielding of unconverted 1ω and 2ω light is complicated.

Program of Work

The program of work included to field experiments that quantify target performance in the areas of laser-plasma interactions, laser-target coupling, preheat and hohlraum filling, and to gain a quantitative understanding of the advantages and limitations of 2ω laser target illumination

relative to 3ω. A limited number of experiments using 2ω light have been documented in the scientific literature in the past. These experiments indicate that laser backscattering levels from laser-plasma instabilities and absorption are similar to those using 3ω. None of these experiments, however, were performed in the plasma conditions and time scales expected for experiments on the NIF, and only a very small number were performed were performed using laser beam smoothing techniques.

The present experiments were performed on a number of laser facilities Omega (LLE), Helen (AWE), Janus (LLNL), and NIF. Although only NIF can deliver the energy required for advanced experiments, significant scientific work in the area of laser-plasma interactions was successfully accomplished on the other facilities. Omega, for example, only has one 2ω beam, but the remaining beams have been used to produce an interaction plasma of high electron temperature and density that approaches the conditions found in NIF target plasmas.

Motivated by the encouraging findings of the present experiments, LLNL is establishing a new capability to allow the exploration of the science of laser matter interactions using 2ω (527 nm) light on a quad of beams on NIF. The addition of a quad of beams operating at 2ω is outside of the current baseline for the NIF project and will have no impact on cost, schedule, or the ability of NIF to meet its milestones and deliverables

Laser-plasma Interactions at 527 nm

1) 2ω diagnostics at Omega

To measure the complete energetics of the 2ω beam when transversing a high-temperature dense plasma a Transmitted Beam Diagnostics (TBD), a Full Aperture BackScatter diagnostic (FABS) and a Near Backscatter Imager (NBI) has been fielded at the Omega laser facility. These diagnostics measure the stimulated Brillouin and Raman backscattered light into and around the focusing lens as well as the transmitted light. We have developed the TBD allowing us to study beam transmission of 2ω light in gas-bag and hohlraum targets for smoothed laser beams. The instrument is an innovative design, that consists of a fused silica curved 3" diameter bare-surface reflector, mounted 23 cm behind target chamber center (tcc) on a remote controlled diagnostic arm installed in one of the target insertion modules. The mirror collects and reflects transmitted light within twice the f/6.7 cone of the original beam through a window to a detector assembly outside the vacuum chamber (Fig. 5). The concave mirror (R=37 cm) focuses the divergent beam behind the target to a focus inside the vacuum chamber and produces a divergent f/13 beam with a diameter of 3.8 cm at the chamber port. An aspheric lens images the TBD collection mirror onto a Lambertian diffuser plate with an optical magnification of 1.7:1.

A second 4 % splitter reflects a small fraction of the beam onto the diffuser plate, while the remaining beam energy is measured in a full aperture calorimeter filtered for 2ω light (Fig. 1). Time integrated two-dimensional near-field images of the transmitted light on the diffuser plate are recorded with a CCD camera through a 2ω bandpass filter (10 nm FWHM). The images show the intensity distribution on the mirror behind the target within 8.5^{o} around the beam axis (twice the inital f/6.7 cone) and are used to measure beam spray and deflection. A fast photodiode (5 GHz bandwidth) records the temporal pulseshape of the transmitted light at 527+/- 5 nm. All three detectors are absolutely calibrated in situ using a low energy (20 J) 2ω laser beam to allow independent measurements of the total transmitted energy.

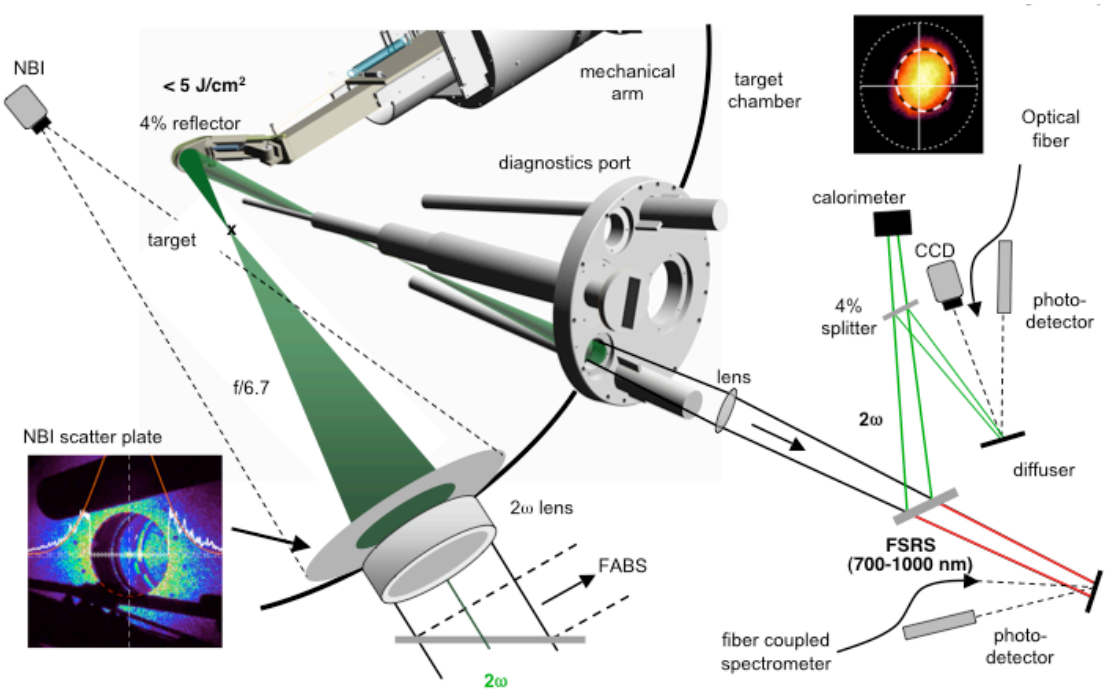

Figure 5. Set-up of the 2ω laser-plasma interaction diagnostics in the Omega target chamber is shown including the FABS, NBI and the TBD. The latter employs a mechanical arm that holds the 4% reflector near the target.

2) Laser-plasma interaction experiments on laser scale-length gasbags

a) Gasbag target platform

Laser-plasma interaction experiments were performed at the Omega laser facility using the 2ω interaction beam and the scattered light diagnostics to emulate the large scale-length plasma conditions that occur in future target physics experiments on the NIF. A large scale length plasma is created by heating a 2.4 mm by 2.75 mm gasbag target with 39 defocused heater beams at 3ω delivering a total energy of 10.5 kJ in a 1 ns square pulse. The hydrocarbon gas filling of the gasbag to about 1 atm results in an electron density n_e around 14% of the critical density for 527 nm light ($n_e = 5.5\ 10^{20}$ cm^{-3}). This corresponds to the current 2ω NIF hohlraum design density.

The heater beams are distributed in 6 different cones on both sides of the target in order to provide maximum homogeneous heating. Gated x-ray images of the heated bag and Thomson-scattering measurements show that a homogeneous plasma is formed after a few 100 ps within the plasma region bounded by the blast wave moving inward due to the ablation of the polyimide skin of the bag. The 1-ns-long probe beam has a variable energy between 20 J and 400 J and is spatially smoothed with a distributed phase plate giving a vacuum spot diameter of about 200 μm and intensity up to $I = 10^{15}$ W cm^{-2}. The 2ω probe beam turns on 500 ps after the start of the heater beams when the plasma is heated to electron temperatures of T_e = 1-2 keV.

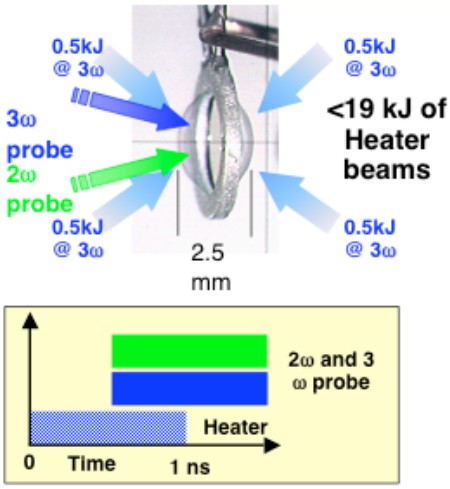

Figure 6. The first target studied were gasbags filled with hydrocarbon gas. We obtained a well-characterized 2 mm-long plasma around T_e=2 keV and 12% of the critical density for 2ω light.

b) Plasma characterization

The temperature of the large-scale length gas bag plasmas through which we studied the 2ω laser beam propagation and laser-target coupling has been measured with Thomson scattering and compared to radiation hydrodynamic modeling. A gasbag consists of a aluminum washer (2.75 mm internal diameter, 0.4 mm thick) with a thin (350 nm) polyimide skin bonded to each side. When inflated with gas at around 1 atm pressure, the skin inflates to form an ellipsoid with a minor axis (of rotation) ≈ 2.4 mm long.

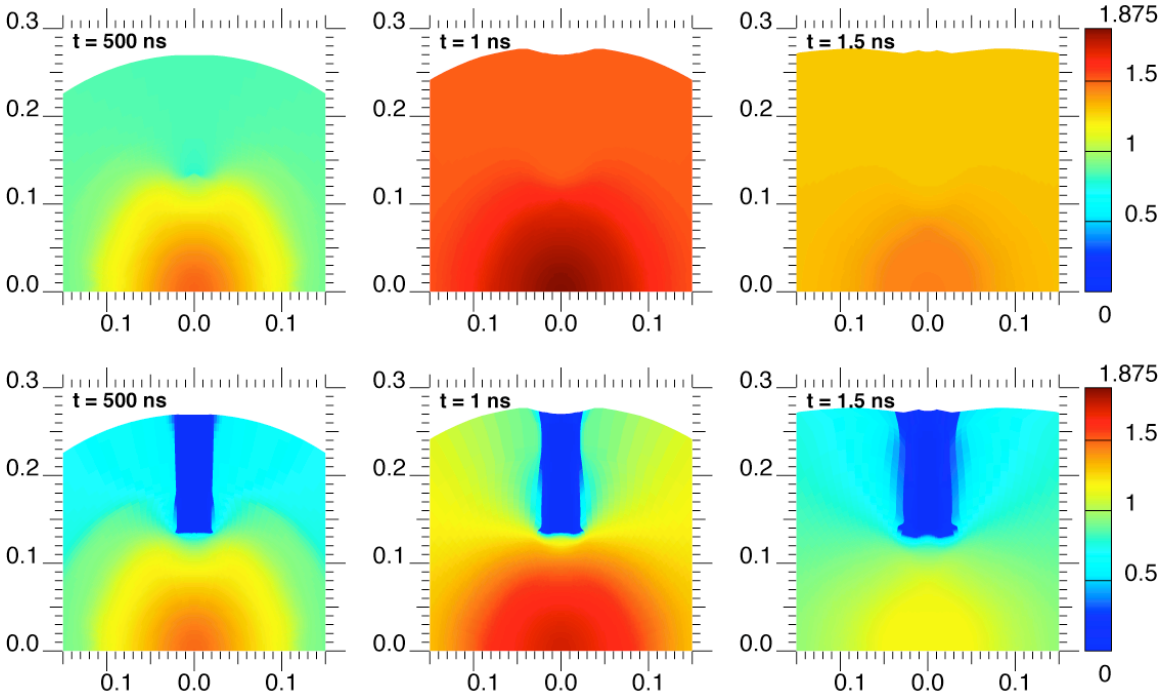

Figure 7. Electron temperature contours from gasbag simulations are shown without (top) and with (bottom) aluminum washer. The axis scales are in cm. The color scale is in keV.

Our analysis includes the aluminum washer that acts as a heat sink to the surrounding plasma and that contributes to rapid cooling of the plasma after the shutoff of the heater beams. In addition, our analysis showed that no aluminum from the inner surface of the washer ablates and moves into the path of the interaction beam affecting its transmission.

Figure 7 compares the electron temperature obtained from our simulations with those performed previously without the aluminum washer. At 0.5 ns, when the interaction beam turns on, the aluminum washer has not significantly impacted the temperature of the gasbag. At 1 ns, when the heater beams turn off, the no-washer simulation has reached its peak temperature of 1.875 keV. Thermal electron conduction to the washer causes the temperature to decrease more rapidly than in the no washer case. By 1.5 ns, as shown in Fig. 7, the peak temperature of the washer simulation is ≈ 250 eV lower than in the no-washer simulation.

By including the effect of the washer in the simulation we also observe excellent agreement with the electron temperature measurements performed with 2ω and 4ω Thomson scattering. Thomson scattering (TS) spectra of the ion-acoustic wave resonances have been obtained at several times, both during the heating and after the driver beams have been turned off. The electron temperature has been extracted from the best fits of experimental spectra using a multi-species TS form factor, assuming $n_e = 5.9\times10^{20}$ cm^{-3} (this density is consistent with the spectrum of the Raman backscattered light) and $T_i \sim T_e/1.5$. The electron temperature is found to approach 1.8 keV during heating ($t < 1$ ns) and drops significantly during the cooling period. Figure 8 compares the experimental data with the HYDRA simulation indicating good agreement when including the Al washer in the simulations. Below we show that detailed features of the beam transmission, the SRS spectra and temporal behavior can be accurately modeled when including the accurate characterization data obtained in this study.

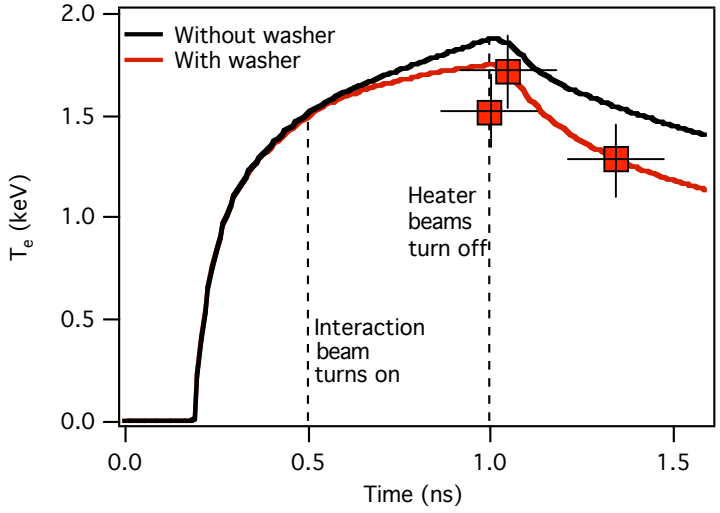

Figure 8. Electron temperature at a distance of r = 85 μm from the gasbag center. Also shown are the results from the Thomson scattering measurements (red squares) showing good agreement when including the washer.

In addition to Thomson scattering on ion acoustic waves, the first Thomson scattering experiment on electron plasma waves in Omega gasbags has indicated scattering from various features of the gasbag plasma. The wavelength of the intense feature measured for 0.5 ns < t < 1

ns is consistent with a scattering feature expected from simulations. This result shows that the SRS instability grows in the density plateau. The goal of the experiments is to mitigate this instability by applying laser beam smoothing techniques and the appropriate laser beam intensities.

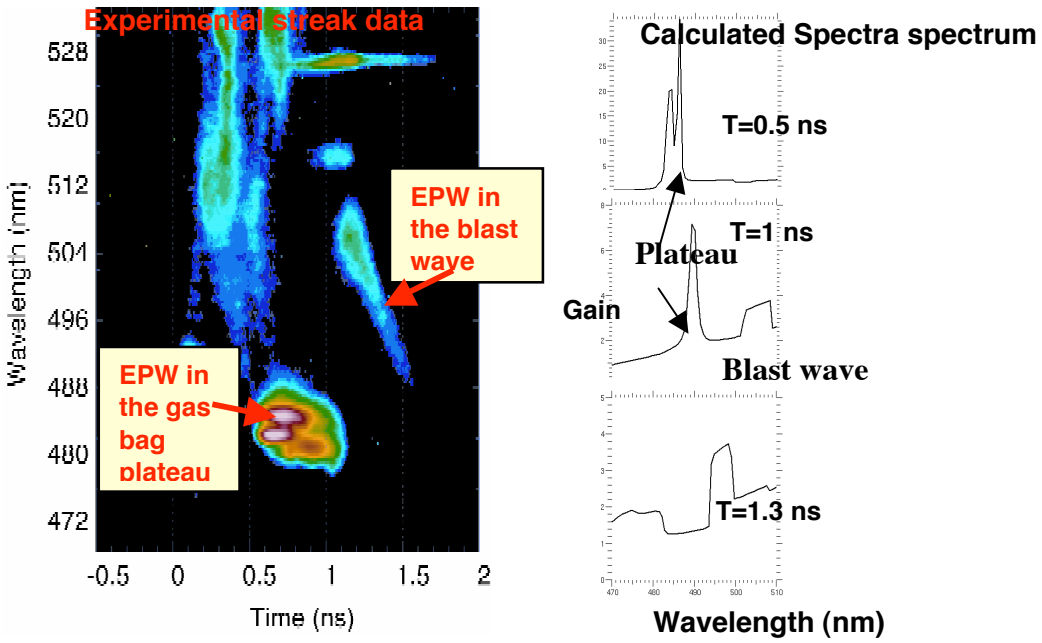

Figure 9. Streak record of Thomson scattered light off the electron plasma wave driven by SRS from the 2ω interaction beam (left) and calculated Thomson scattering spectra from LIP and plasma conditions from LASNEX (right).

Figure 9 shows the experimental spectra and calculated spectra. The latter clearly reproduce the wavelength of the scattering feature at 480 - 490 nm. At t = 1 ns, this feature disappears. This observation can be interpreted with a suppression of the instability by the arrival of the blast wave. The arrival time of t = 1 ns is predicted by radiation hydrodynamic LASNEX modeling and also consistent with 2-D x-ray imaging. At t > 1 ns, we find scattering at the wavelength l ~ 500 nm that can also be reproduced by our calculated spectra.

c) Mitigation of beam spray with smoothing by spectral dispersion at 527 nm

A primary objective of the Omega experimental campaigns was to show that good propagation of a 2ω high intensity laser beam through a large-scale hot plasma can be obtained. For that purpose, we used Omega beam smoothing capabilities, which are similar to those of NIF. In addition to spatial smoothing using phase plates, the interaction beam can be temporally smoothed by spectral dispersion (SSD) by applying an oscillating RF field to an electro-optic crystal that modulates the phase of the seed laser pulse. This adds up to 11 Å bandwidth (at 1 μm) to the narrow linewidth of the laser which is then dispersed with a grating.

Figure 10 shows measured near-field images of the interaction beam for various intensities. At an intensity of 10^{15} Wcm^{-2}, the beam exhibits a large spray outside the initial f/6.7 cone (dashed inner circle) reaching the edge of the diagnostic sensitive area defined by the size of the TBD mirror (dotted outer circle). When 11 Å SSD is applied, the beam spray is reduced considerably (II). As a reference, Fig. (III) shows a low intensity calibration shot without plasma where the

beam stays within the f/6.7 cone. At an intensity of 5 10^{14} Wcm^{-2}, beam spray is still visible (IV). Both 5 and 11 Å SSD provides a similar reduction in spray (V). At much lower intensity (1.5 10^{14} Wcm^{-2}) beam spray becomes negligible (VI).

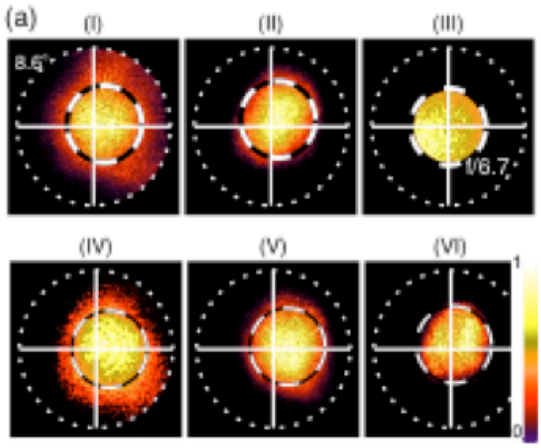

Figure 10. Near-field images of a 10^{15} W cm^{-2} interaction beam without (I) and with 11 Å SSD (II) are shown. The images in (IV) and (V) are the corresponding images for a lower intensity of 5 10^{14} W cm^{-2}. We also show a low intensity (1.5 10^{14} W cm^{-2}) shot with 5 Å SSD (VI) and a low energy calibration shot without plasma (III). The cross defines the center of the TBD mirror while the dashed circle represents an f/6.7 cone (4.3°) around the transmitted beam centroid.

Averaged radial intensity profiles [Fig. 11] around the center of the deflected beam quantify the fraction of energy inside a solid angle defined by its half-cone angle φ. Figure 11 shows the fraction of transmitted energy inside the original f/6.7 cone as a function of intensity and temporal smoothing. At the highest intensities, only a third of the energy of the unsmoothed beam is contained inside the f/6.7 cone. With SSD it increases to 50%, reaching more than 80% for lower intensities (1.5 10^{14} Wcm^{-2}). At high intensities, when the beam spray is large enough to exceed the f/3.3 TBD collection mirror, a smooth fit to the wings of the intensity profile is applied to estimate the beam intensity distribution outside the mirror (φ > 8.6°). For an unsmoothed beam at 10^{15} Wcm^{-2} roughly 20% of the beam energy is outside the collection mirror. The error bars indicate the variation of beam spray for different directions (horizontal to vertical) due to the asymmetry of the spray.

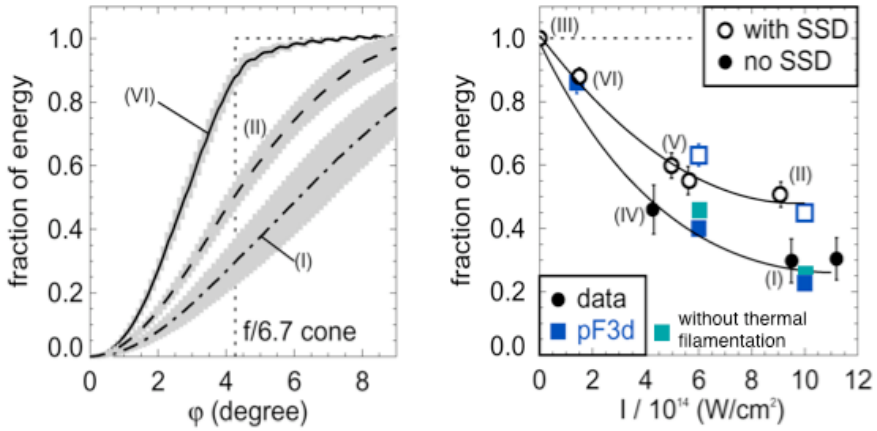

Figure 11. (left) Fraction of beam energy within the angle φ around the beam center corresponding to Fig. (I), (II) and (VI). (right). Fraction of energy is shown inside the initial

f/6.7 cone as a function of beam energy and temporal smoothing and comparison with the modeling. The lines are simple fits to the data.

Figure 11 shows that for our plasma conditions, the spray of the 2ω interaction beam is controlled by either reducing its intensity around 2 10^{14} Wcm^{-2} or adding up to 11 Å of SSD bandwidth. These intensities are consistent with present 2ω ignition hohlraum designs. This is an encouraging result because the suppression of filamentation by SSD will ensure that the laser beams illuminate the hohlraums walls in a controlled and predictable way to achieve symmetric capsule implosions.

Two-dimensional (2D) cylindrical hydrodynamic simulations done with the code HYDRA, using a realistic beam pointing and focusing, give the evolution of the plasma density and temperature. A peak electronic temperature T_e = 1.8-2 keV is predicted in the 2 mm long density plateau (n_e = 5.5 10^{20} cm^{-3}). Hydrodynamic profiles at 0.8 ns and 1.2 ns (the interaction beam is on from 0.5 ns to 1.5 ns) were used as input for more detailed laser-plasma interaction simulations, using pF3d. The calculations include a coupled-wave model of backscattering instabilities with a nonlinear hydrodynamic module and a model for nonlocal heat conduction. Ponderomotive and thermal filamentation are thus naturally present, driving density perturbations resulting in refraction, diffraction and beam spray. The simulations were done in a 2D-planar geometry, using the measured focal spot shape and a realistic model of spatial and temporal smoothing.

The calculated beam spray is shown in Fig. 11 (right). The error bars correspond to the uncertainty in plasma parameters from the HYDRA simulations (by comparing various heat conduction models) and their evolution between 0.8 and 1.2 ns. The threshold and increase in beam spray with intensity is well reproduced, as well as the strong beneficial effect of temporal smoothing.

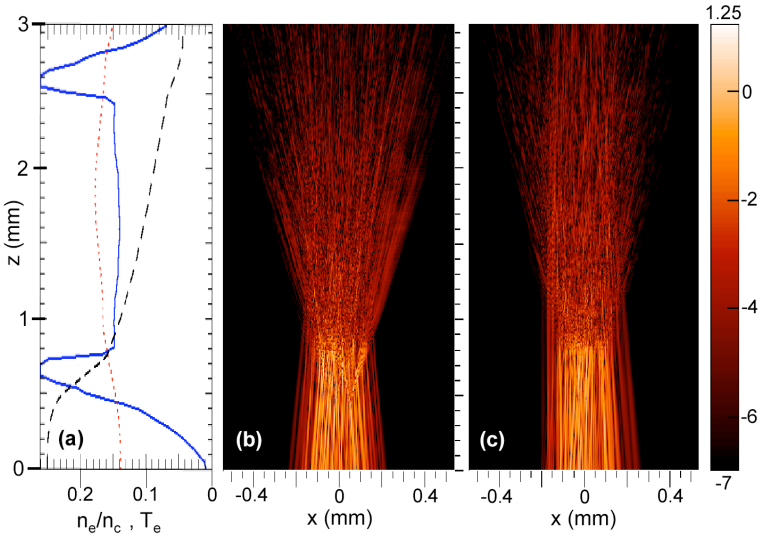

Figure 12. Calculations with the code pF3D show the 2ω interaction beam propagating through the gasbag plasma. The intensity is 10^{15} Wcm^{-2}. (a) Plasma conditions from HYDRA. (b) Beam propagation without SSD. (c) Improved propagation with 11 Å (1ω) of SSD.

Figure 12 shows the propagation of the interaction beam through the plasma. Most of the filamentation and spray occurs in the blast wave first traversed by the interaction beam, around z = 0.7 mm. In this short (200 μm) and dense ($n_e \sim 10^{21}$ cm^{-3}) [Fig. 12 (a)] plasma, a significant fraction of the speckles generated by the phase plate are above their critical power for self-focusing when the average intensity reaches 2-3 10^{14} Wcm^{-2}, consistent with the onset of beam spray seen in Fig. 12. Thermal filamentation contributes also to the beam spray. A simulation where thermal effects are turned off and only ponderomotive filamentation is considered [with laser parameters corresponding to Fig. 10 (IV)] shows 50% of the energy inside the f/6.7 cone versus 40% when thermal effects are included. Indeed, the electron mean free path in the blast wave is $\lambda_{ei} \sim 8$ μm, comparable to a speckle width $2f\lambda_0 \sim 6$ μm, which suggests that heat conduction will not smooth out temperature (and therefore density) perturbations. It should be noted that at the highest intensity, the maximum local temperature perturbation reaches 35%, certainly close to the limit of validity for pF3d's (linear) nonlocal heat conduction model.

Also, these 2D simulations could overestimate the beam spray, as the lost transverse degree of freedom leads to larger density and temperature perturbations. A multiplier on the local intensity is used to recover the correct average intensity as the beam propagates [i.e. reproducing the three dimensional (3D) Rayleigh length]. As the critical power for ponderomotive filamentation of a speckle is the same (within 20%) in 2D or 3D, we expect good agreement between our 2D modeling and measurements done near ponderomotive filamentation threshold (i.e. for measurements around 4 10^{14} $W.cm^{-2}$). As three-dimensional simulations of these large targets are not practical with current computers, simulation results at higher intensity are our best estimate, but we can not rule out a different result in 3D.

In order to assess the efficiency of SSD in reducing beam spray, we estimate the time a speckle needs to create a density hole to be the transit time of an ion acoustic wave traveling at the speed of sound ($C_s \sim 0.4$ $\mu m.ps^{-1}$ for our plasma conditions) through an f/6.7 speckle $T_{trans} = f\lambda_0/C_s \sim 9$ ps. This can be compared with the lifetime of a speckle, given by the laser correlation time T_{corr} = 3.4 (1.7) ps for 5 (11) Å of SSD bandwidth at 1.053 μm. This is consistent with the strong reduction of beam spray measured when several Å of SSD bandwidth are used as T_{corr} becomes much shorter than T_{trans}.

d) Absolute transmission and backscatter at 527 nm

Besides beam spray, the TBD measures the absolute interaction beam transmission. It decreases with intensity from 20% at 1.5 10^{14} Wcm^{-2} to 6% at 10^{15} $W.cm^{-2}$ (Fig. 8). The error bars indicate the variation of experimental results obtained independently with the calorimeter, the diode and the CCD camera and include the intrinsic precision of each instrument. At the highest intensities around 10^{15} $W.cm^{-2}$ where the beam spray is large enough to exceed the f/3.3 TBD collection mirror the total beam transmission can be up to 20% higher than the measured value, which is within the error bars of the measurement.

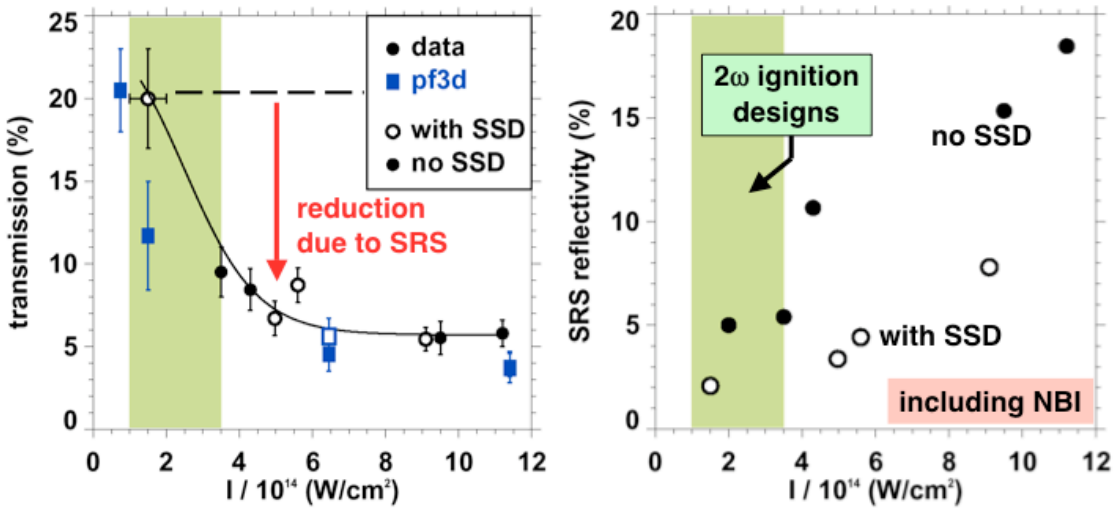

Figure 13. (left) Measured beam transmission as a function of intensity with and without SSD (circles) and comparison with pF3d calculations (boxes). (right) measured SRS reflectivity as a function of intensity with and without SSD. SSD affects mainly SRS originating from the blow-off in front of the density plateau and the effect is within the error bar of the transmission measurements.

We find that the measured transmitted energy fraction of the 2ω beam is independent of SSD. The (time-averaged) inverse bremsstrahlung absorption calculated with HYDRA is ~ 0.75-0.85, in agreement with the measured transmission at low intensity. Figure 13 shows that pF3D also reproduces the decrease of the transmission with increasing intensity. This is due to stimulated Raman backscattering (SRS) originating from the density plateau, of up to 30% for the highest intensity. The SRS threshold is found around 10^{14} W cm^{-2}, leading to the large error of 30% in the calculated transmission around this intensity.

The full aperture backscatter measurements of Brillouin and Raman backward scattered light show only modest amounts of SRS (well below the peak 30% SRS seen in simulations in the density plateau), as strong re-absorption occurs in the blast wave. While SSD strongly reduces the beam spray, it only marginally affects SRS, as the instability develops on a much faster time scale (< 1ps) than filamentation (~ 10 ps). While SSD reduces the measured SRS fraction, it is less than a 5% contribution to the overall energy balance and thus doesn't affect the measured transmission through the gasbag. pF3D simulation have shown that the measured SRS comes from the density ramp in the blow-off before the density plateau, where T_e is much lower and filamentation is active in speckles. Our simulation reproduce well the observed thresholds and trends seen with various beam smoothing combinations. This will be the object of a forthcoming publication.

The Omega gasbag experiments shown that the spray of the 2ω interaction beam in an ignition scale plasma is controlled by reducing its intensity to a few times 10^{14} Wcm^{-2}. Adding up to 11 Å of SSD bandwidth allows a factor of two higher intensities while keeping the beam spray constant. Our fluid laser plasma interaction modeling is in good agreement with these results. This suggests that future experiments using 527 nm light and large scale-length plasmas where beam propagation is critical should stay in this range of intensities. The agreement between these observations and the modeling further indicates that scaling to different density, temperature, and aperture conditions can be reliably performed.

3) Effect of target materials on hot electron production by 2ω laser plasma interactions

The sensitivity of the laser-plasma interactions to the choice of materials has been investigated in gasbag experiments that have been performed on the HELEN laser. The studies measure 2ω laser-beam propagation and stimulated Raman backscattering. Eleven gasbag targets filled with neopentane gas were shot with varying amounts of krypton dopant. The total SRS backscatter and time-resolved SRS spectra were recorded for each shot.

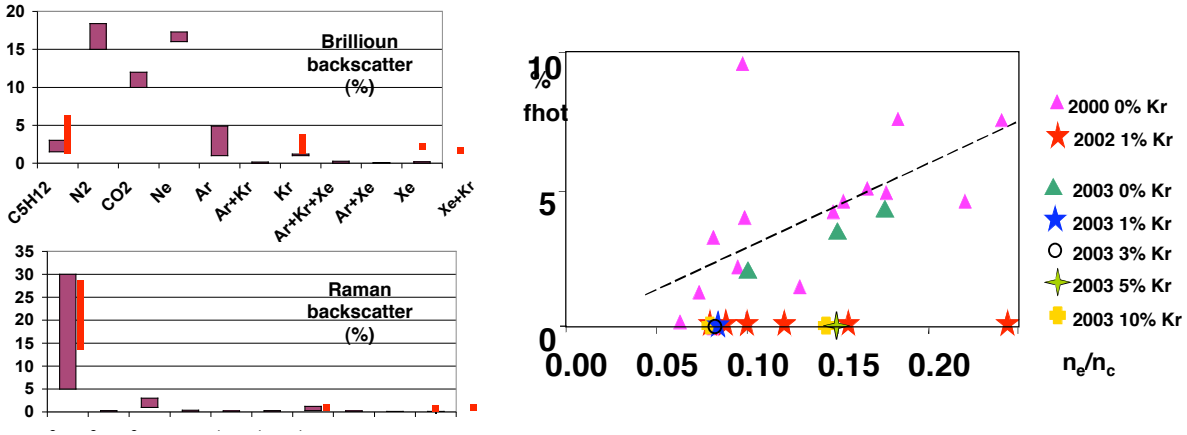

Figure 14. SBS and SRS laser backscattering from the 2ω interaction beam through the gasbag (left). Also shown is the hot electron production for the C_5H_{12}-filled gas bag targets that produce the largest SRS scatter of up to 30%. Small fractions of Kr impurities have been added for some shots yielding to a reduction of the hot electron fraction by one order of magnitude (right).

Figure 14 shows the measurements of SBS and SRS backscatter as a function of plasma composition. Further composition experiments were performed on the Helen laser in late summer. These experiments show the surprising findings that very small amounts of Kr dopant in a C_5H_{12} plasma (a Stimulated Raman Scattering (SRS) producer) can significantly reduce the hot electron production. Figure 11 summarizes measurements of the hot electron fraction, f_{hot}, in Helen gasbags (right). Gasbags without Kr show a hot electron production that rises with density. Adding a small amount of Kr appears to quench hot electron production in these targets. The data shown includes the data over several years including the experiments performed in this period, which reproduced the earlier findings. An interpretation of these experiments is that a surprisingly tiny fraction of dopant can have a very large effect the saturation of electron waves. These composition studies are the result from a collaboration with the Atomic Weapons Establishment, UK.

4) Laser-plasma interaction at 527 nm in high electron temperature hohlraum plasmas

a) High electron temperature hohlraum target platform at $T_e = 3.5$ keV

The maximum electron temperature in gasbags is limited at Omega to $T_e = 2$ keV due to the open geometry of the target and the limited amount of energy that can be fired with opposing heater beams (as the plasma quickly becomes transparent). To reach NIF-like temperature $T_e > 3$ keV, we have developed a new target platform. A 2-mm-long, 1.6 diameter gold hohlraum is filled with a 1 atm mix of hydrocarbon gas, producing a millimeter-size density plateau around $n_e = 5$

10^{20} cm^{-3}. 36 heater beams can deposit up to 16 kJ of energy in 1 ns inside the target, leading to a peak temperature on axis around 3.5 keV. The 2ω interaction beam is then fired along the hohlraum axis, which allow for all the 2ω diagnostics (TBD, FABS, NBI).

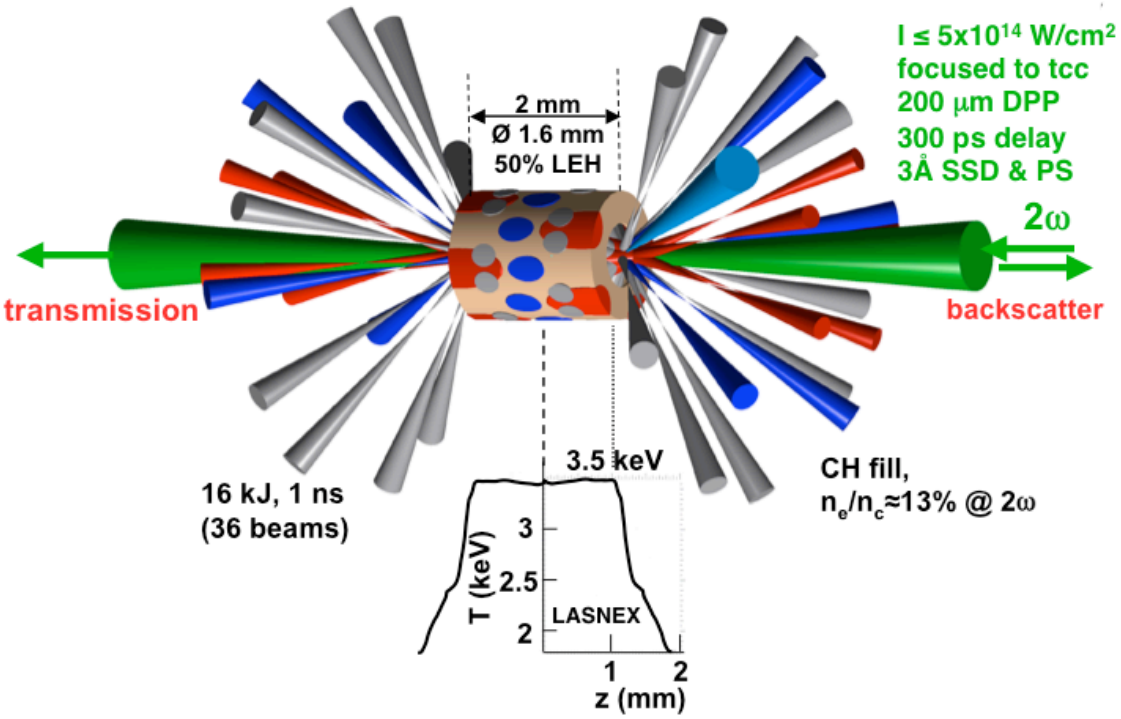

Figure 15. Using a closed geometry (hohlraum) allows E_{LASER} > 16 kJ of heater beam energy deposited into the target. Electron temperatures of T_e = 3.5 keV are reached.

b) Plasma characterization with Thomson scattering

To validate this target platform, the temperature has been measured with 4ω Thomson scattering at target chamber center.

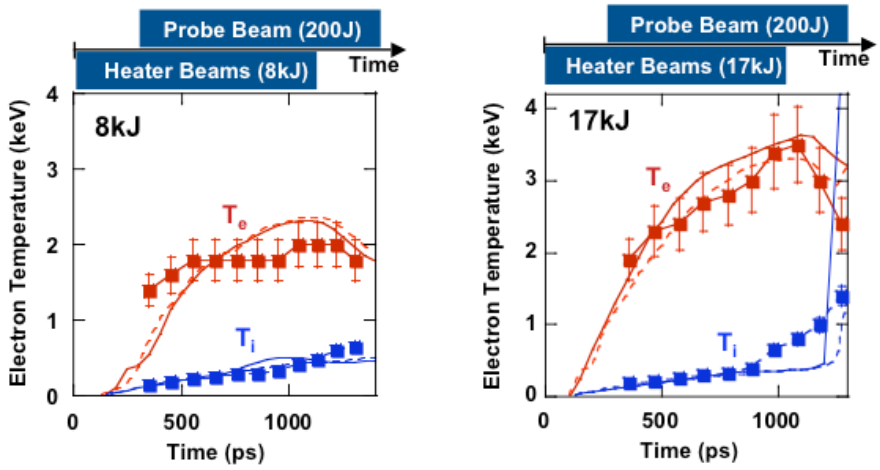

Figure 16. 4ω Thomson scattering has been applied demonstrating high electron temperatures in agreement with radiation-hydrodynamic simulations (square data). The solid curves shows HYDRA code predictions using a f=0.05 heat transport flux limiter. The ion temperature is measured to rise faster than simulated after 1 ns due to on-axis stagnation of the plasma.

Figure 16 shows the experimental results compared with simulations using the code HYDRA. Using a multispecies plasma (CH) allows for an independent measurement of the electron (T_e) and ion (T_i) temperatures. The agreement is very good up until 1 ns when the plasma begins to accumulate on axis (stagnation) and the simulations begin to underestimate T_i. As shown in Fig. 16, we can control the electron temperature by varying the amount of heater beam energy, thus bridging the gap between the gasbags experiments (T_e < 2 keV) and the hottest hohlraums (T_e > 3.5 keV) such as on NIF.

c) Scaling of transmission and backscatter with electron temperature and laser intensity

The hohlraum targets were heated with a total energy of 8kJ to 15 kJ in a 1 ns flat-top pulse, distributed in three cones around the hohlraum axis. The green interaction beam was delayed by 300 ps relative to the heater beams and smoothed with a combination of PS, SSD (3Å) and a DPP that resulted in a 200 μm focal spot. We heave measured a total beam transmission of up to 80% in CH-filled hohlraum targets at 2ω intensities of $3x10^{14}$ W/cm^2 and densities of n_e/n_c=6% (at 3ω). Simultaneously we have observed negligible SRS reflectivity but SBS levels up to 25% (these values include the light scattered outside the lens onto the NBI scatter plate). When the heater energy is reduced from 15 kJ to 8 kJ and the plasma temperature is reduced from 3.5 keV to 2 keV, the total beam transmission decreases to 25%.

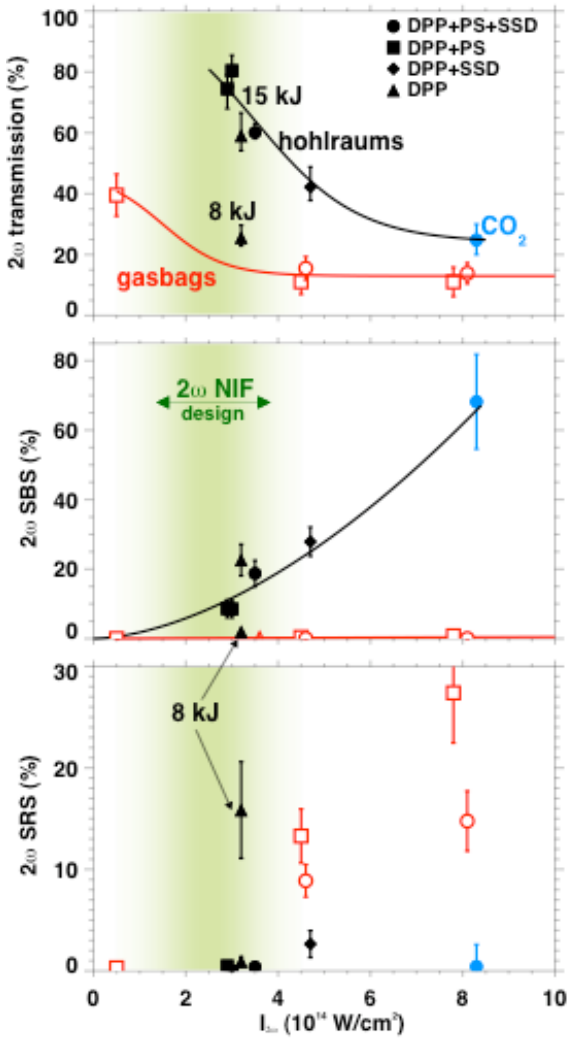

In the 2keV regime we measure a SRS reflectivity around 15% with no SBS. This is consistent with earlier experiments on gasbag-plasmas with a temperature of only 1.8 keV, where we also observe modest levels of SRS but negligible SBS. Temporally resolved spectra of the 2ω and 3ω backward and forward Broulouin scattered light show spectral shifts consistent with the peak temperatures inferred from Thomson scattering indicating that the scattering occurs in the bulk of the plasma. (Fig. 18).

Figure 17. Beam transmission, SBS and SRS vs. intensity for hohlraums conditions with temperatures ranging from 2 keV to 3.5 keV (full symbols) and 1.8 keV gasbags (open symbols).

With increasing 2ω laser beam intensities, above the current 2ω NIF ignition hohlraum designs ($8x10^{14}$ W/cm^2), the transmission decreases to 25% as the SBS reflectivity increases to ~70%.

These findings suggests that 2ω scattering losses at 2ω ignition-relevant hohlraum plasma electron temperatures are suppressed by "Landau" damping of collective plasma oscillations initially set-up by the intense laser field-plasma interaction. We can therefore expect that existing modeling calculating adequate 2ω beam propagation in ignition hohlraums on NIF will be valid. With best laser smoothing conditions including phase plates (CPPs), polarization smoothing (PS), and smoothing by spectral dispersion (SSD), the new database indicates that experiments with 2w laser beam intensities of $3x10^{14}$ W/cm^2 will provide propagation and coupling.

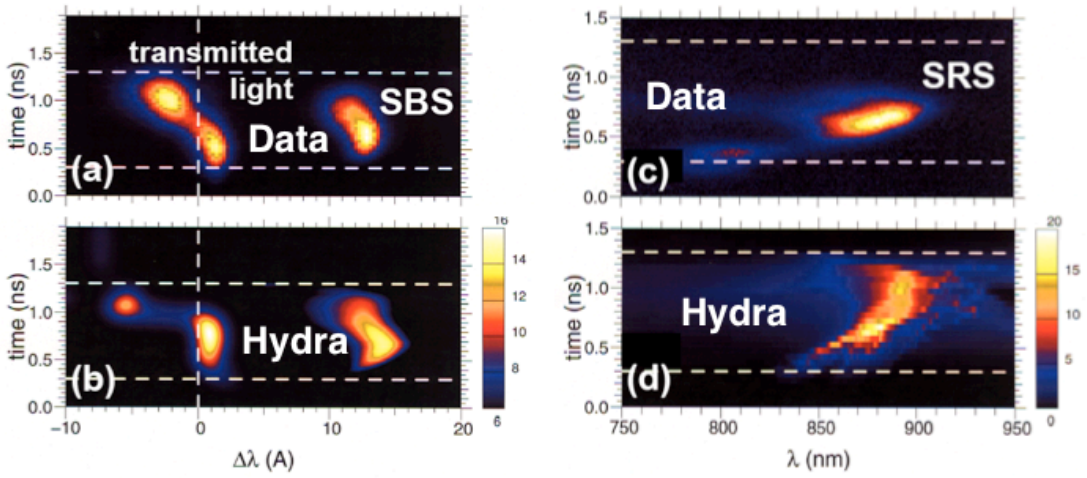

Figure 18. The backscattered Brillouin (left) and Raman (right) spectra are compared to post-processed HYDRA simulations. When the blue shift due to time-transit effects on the transmitted light is included, the good agreement shows that the 2ω beam interacts with a 3.5 keV, 13% crit plasma.

This work was performed under the auspices of the U. S. Department of Energy (DOE) by the University of California, Lawrence Livermore National Laboratory (LLNL) under Contract No. W-7405-Eng-48. The project 03-ERD-071 was funded by the Laboratory Directed Research and Development Program at LLNL.

Publications

1. UCRL-CONF-203442
   Transmitted laser beam diagnostic at the Omega laser facility,
   C. Niemann, G. Antonini, S. Compton, S. H. Glenzer, D. Hargrove, J. D. Moody, R. K. Kirkwood, V. Rekow, C. Sorce, W. Armstrong, R. Bahr, R. Keck, G. Pien, W. Seka, K. Thorp,

   Review of Sci. Intrum. 75, 4171 (2004).

2. UCRL-JRNL-202679
   Intensity Limits for Propagation of 0.527 μm Laser Beams through Large-Scale-Length Plasmas for Inertial Confinement Fusion,
   C. Niemann, L. Divol, D.H. Froula, G. Gregori, R. K. Kirkwood, A. J. MacKinnon, N. B. Meezan, J. D. Moody, C. Sorce, L. J. Suter, R. Bahr, W. Seka, S. H. Glenzer,

   Phys. Rev. Lett. 94, 085005 (2005).

3. UCRL-CONF-201547
   A summary of explorations into the use of green light for high-gain, high-yield experiments on the National Ignition Facility
   L. J. Suter, S. H. Glenzer, S. Haan, B. A. Hammel, K. Manes, N. Meezan, J. D. Moody, M. Spaeth, K. Oades, M. Stevenson,
   Nucl. Fusion **44** (2004) S140-S148.

4. UCRL-JRNL-201543
   Prospects for high-gain, high yield NIF targets driven by 2ω (green) light,
   L. J. Suter, S. Glenzer, S. Haan, B. Hammel, K. Manes, N. Meezan, J. Moody. M. Spaeth, L. Divol, K. Oades, M. Stevenson,
   Phys. Plasmas **11**, 2738-2745 (2004).

5. UCRL: will be provided
   Effects of plasma composition on backscatter and hot electron production in underdense plasmas,
   R.M. Stevenson, L. J. Suter, K. Oades, W. L. Kruer, G. Slark, B.R. Thomas, R. L. Kauffman, M. Miller, S. Glenzer, J. Moody, C. Niemann, J Grun, J Davis, C. Back, B. Thomas,
   Phys. Plasmas **11**, 2709-2715 (2004).

6. UCRL-JC-143413
   The physics basis for ignition using indirect-drive targets on the National Ignition Facility,
   J. D. Lindl, P. Amendt, R. L. Berger, S. G. Glendinning, S. H. Glenzer, S. W. Haan, R. L. Kauffman, O. L. Landen, and L. J. Suter,
   Phys. Plasmas **11**, 339-491 (2004).

7. UCRL-JC-152243
   Effects of ion trapping on crossed-laser-beam stimulated Brillouin scattering,
   E. A. Williams, B. I. Cohen, L. Divol, M. R. Dorr, J. A. Hittinger, D. E. Hinkel, A. B. Langdon, R. K. Kirkwood, D. H. Froula, and S. H. Glenzer,
   Phys. Plasmas **11**, 231-244 (2004).

5. UCRL-PRES-203916
   Direct observation of the saturation of stimulated Brillouin scattering by ion-trapping induced frequency shift,
   D.H. Froula, L. Divol, A. A. Offenberger, N. Meezan, T. Ao, G. Gregori, C. Niemann, D. Price, C. A. Smith, and S. H. Glenzer,

   Phys. Rev. Lett. **93**, 035001 (2004).

6. UCRL-JRNL-155615
   Observation of the parametric two-ion decay instability with Thomson scattering'
   C. Niemann, S.H. Glenzer, J. Knight, L. Divol, E.A. Williams, G. Gregori, B.I. Cohen, C. Constantin, D.H. Froula, D.S. Montgomery, R.P. Johnson,

   Phys. Rev. Lett. **93**, 045004 (2004).

7. UCRL-CONF-203798
   Calibration of Initial Measurements from the Full Aperture Backscatter System on NIF;
   R. K. Kirkwood, T. Mccarville, D. H.Froula, B. Young, D. Bower, N. Sewall, C. Niemann, M. Schneider, J. Moody, G. Gregori, F. Holdener, M. Chrisp, B. J. MacGowan, S. H. Glenzer and D. S. Montgomery,
   accepted in Review of Sci. Intrum. (2004).

8. UCRL-JRNL-203525
   Saturation of Power Transfer Between Two Co-Propagating Laser Beams by Ion Wave Scattering in a Single-Species Plasma; R. K. Kirkwood, E. A. Williams, B. I. Cohen, L. Divol, M. R. Dorr, J. A. Hittinger, A. B. Langdon, C. Niemann, J. Moody, L. J. Suter, O. L. Landen,
   submitted to Phys. Rev. Letters (2004).

9. UCRL-JC-152993:
   Implementation of a high-energy 2ω probe beam on the Omega laser
   A.J.Mackinnon, S. Shiromizu, G. Antonini, K. Haney, D.H Froula, J. Moody, G. Gregori, K. Campbell, C.Sorce, L.Divol, R. L. Griffith, S. Glenzer
   accepted in Review of Sci. Intrum. (2004).

10. UCRL-CONF-203615:
    Implementation of high-energy 4ω Thomson-scattering diagnostic beam on the Omega laser,
    A.J.Mackinnon, G.Gregori, R. Huff, J.Armstrong, K.Thorp, D. Froula, J. Moody, R.Bahr, C.Sorce, S. Shiromizu, J. Dressler, J. Satariano, G. Antonini, K.Haney, J. Zumstein, W.Seka, D. Meyerhofer, S. Loucks, S. Glenzer,

    accepted in Review of Sci. Intrum. (2004).

11. UCRL-CONF-155301
    Progress in Long Scale Length Laser-Plasma Interactions
    S. H. Glenzer and NIF team,
    in Inertial Fusion Sciences Applications eds. B. A. Hammel, D. D. Meyerhofer, J. Meyer-ter-Vehn, H. Azechi (American Nuclear Society, La Grange Park, 2003), pp. 207-212.

12. UCRL-JC-152367
    Experimental Studies of Simultaneous, 351 nm and 527 nm Laser Beam Interactions in a Long Scalelength Plasma,
    J. D. Moody, L. Divol, S. H. Glenzer, A. J. Mackinnon, D. H. Froula, G. Gregori, W. L. Kruer, L. J. Suter, E. A. Williams, R. Bahr, and W. Seka,
    in Inertial Fusion Sciences Applications eds. B. A. Hammel, D. D. Meyerhofer, J. Meyer-ter-Vehn, H. Azechi (American Nuclear Society, La Grange Park, 2003), pp. 218-222.

13. UCRL-JC-151573:
    Self Thomson Scattering in Laser Produced Plasmas,
    C. Niemann, S. H. Glenzer, R. L. Kauffman, N. B. Meezan, M. Miller, K. Oades*, G. Slark* M. Stevenson* and L. J. Suter,
    in Inertial Fusion Sciences Applications eds. B. A. Hammel, D. D. Meyerhofer, J. Meyer-ter-Vehn, H. Azechi (American Nuclear Society, La Grange Park, 2003), pp. 276-279.

14. UCRL-JC-151256:
Stimulated Brillouin Scattering from Helium-Hydrogen Plasmas,
D. H. Froula, L. Divol, D. Price, R. Griffith, G. Gregori, E. A. Williams and S. H. Glenzer,
in Inertial Fusion Sciences Applications eds. B. A. Hammel, D. D. Meyerhofer, J. Meyer-ter-Vehn, H. Azechi (American Nuclear Society, La Grange Park, 2003), pp. 280-282.

15. UCRL-JC-151308:
Blue and Green Light? Wavelength Scaling for NIF,
William Kruer, John Moody, Larry Suter, Siegfried Glenzer, A. Mackinnon, D. Froula, G. Gregori, L. Divol and M. Miller, R. Bahr, W. Seka, Kevin Oades, and R. M. Stevenson,
in Inertial Fusion Sciences Applications eds. B. A. Hammel, D. D. Meyerhofer, J. Meyer-ter-Vehn, H. Azechi (American Nuclear Society, La Grange Park, 2003), pp. 223-237.

16. UCRL-PRES-151995
Prospects for high-gain, high yield NIF targets driven by 2ω (green) light,
L. J. Suter, S. Glenzer, S. Haan, B. Hammel, K. Manes, N. Meezan, J. Moody, M. Spaeth, and L. Divol,
in Inertial Fusion Sciences Applications eds. B. A. Hammel, D. D. Meyerhofer, J. Meyer-ter-Vehn, H. Azechi (American Nuclear Society, La Grange Park, 2003), pp. 223-237.